Revista Mexicana de Astronomía y Astrofísica, **53**, 1–16 (2017)

ABUNDANCES IN PHOTOIONIZED NEBULAE OF THE LOCAL GROUP AND NUCLEOSYNTHESIS OF INTERMEDIATE MASS STARS

W. J. Maciel,[1] R. D. D. Costa,[1] and O. Cavichia[2]

Received December 13 2016; accepted January 27 2017

RESUMEN

Las nebulosas fotoionizadas, incluyendo regiones HII y nebulosas planetarias, son excelentes laboratorios para investigar la nucleosíntesis y la evolución química de varios elementos, en nuestra galaxia y en galaxias del Grupo Local. En este trabajo: (i) comparamos las abundancias en regiones HII y nebulosas planetarias para investigar las diferencias que se derivan de las edades y el origen de estos objetos; (ii) comparamos la evolución química en distintos sistemas, como la Vía Láctea, las Nubes de Magallanes y otras galaxias del Grupo Local; (iii) investigamos qué tanto la contribución de las estrellas progenitoras a la nucleosíntesis afecta las abundancias observadas en las nebulosas planetarias, lo cual constriñe la nucleosíntesis de estrellas de masa intermedia. Mostramos que todos los objetos estudiados presentan tendencias similares en cuanto a las correlaciones independientes de las distancias, y encontramos que pueden definirse límites a la producción de He y N en las estrellas progenitoras de las nebulosas planetarias.

ABSTRACT

Photoionized nebulae, comprising HII regions and planetary nebulae, are excellent laboratories to investigate the nucleosynthesis and chemical evolution of several elements in the Galaxy and other galaxies of the Local Group. Our purpose in this investigation is threefold: (i) compare the abundances of HII regions and planetary nebulae in each system in order to investigate the differences derived from the age and origin of these objects, (ii) compare the chemical evolution in different systems, such as the Milky Way, the Magellanic Clouds, and other galaxies of the Local Group, and (iii) investigate to what extent the nucleosynthesis contributions from the progenitor stars affect the observed abundances in planetary nebulae, which constrains the nucleosynthesis of intermediate mass stars. We show that all objects in the samples present similar trends concerning distance-independent correlations, and some constraints can be defined on the production of He and N by the PN progenitor stars.

Key Words: galaxies: abundances — Galaxy: disk — ISM: abundances — planetary nebulae: general

1. INTRODUCTION

Planetary nebulae (PN) have strong emission lines of H, He, O, N, Ne, S, and Ar, including forbidden lines and recombination lines. The analysis of these lines gives abundances accurate to about 0.2 to 0.3 dex. The abundances include elements that are probably not significantly produced by the progenitor stars (O, S, Ne, Ar), and therefore contribute to the study of the chemical evolution of the host galaxies. The abundances of these elements in planetary nebulae are not expected to be affected in a signficant way by the evolution of their progenitor stars. In fact, the average abundances of these elements are not very different from the observed abundances in HII regions. The same is true for the correlations of the ratios Ne/H, Ne/O, etc. with the metallicity, as measured by the O/H ratio. Therefore, the measured abundances of these elements in PN reflect the interstellar abundances at the time the

[1]Instituto de Astronomia, Geofísica e Ciências Atmosféricas, Universidade de São Paulo, Brazil.
[2]Instituto de Física e Química, Universidade Federal de Itajubá, Brazil.

progenitor stars were formed, and can be compared with the abundances of red giants, AGB stars, and younger objects, such as HII regions and Blue Compact Galaxies (BCG), provided the age-metallicitiy relation and the presence of abundance gradients, both radial and vertical, are taken into account.

Planetary nebulae also provide accurate abundances of some elements that are produced by the progenitor stars (He, N, C), so that the analysis of these abundances and their distance independent correlations can be used to test nucleosynthesis predictions of theoretical models for intermediate mass stars.

Some of these elements are difficult to study in stars, and are better observed in photoionized nebulae. In fact, in recent years there has been an important advance in the determination of accurate abundances in PN and in HII regions, both in the Milky Way and in several external galaxies, particularly in the Local Group. Blue Compact Galaxies (BCG) and Emission Line Galaxies (ELG) can also be included as low metallicity HII regions, as we will see in the following sections. In this work, we consider the abundances of several chemical elements in PN based on our own results and on some recent data from the literature, and compare these results with the abundances of HII regions, Blue Compact Galaxies, and Emission Line Galaxies both in the Galaxy and in other objects of the Local Group. Our purpose in this investigation is threefold: (i) compare the abundances of HII regions and PN in each system in order to investigate the differences derived from the age and origin of these objects, (ii) compare the chemical evolution in different systems, such as the Milky Way, the Magellanic Clouds, and other galaxies of the Local Group, and (iii) investigate to what extent the nucleosynthesis contributions from the progenitor stars affect the observed abundances in planetary nebulae, which constrains the nucleosynthesis of intermediate mass stars.

2. THE DATA

The data used in this investigation include a large sample of PN and HII regions in the following galaxies: The Milky Way (MW), the Large Magellanic Cloud (LMC), the Small Magellanic Cloud (SMC), M31, M32, M33, M51, M81, M101, NGC 185, NGC 205, NGC 300, NGC 628, NGC 3109, and the Sextans galaxy. Typical uncertainties in the abundances are 0.2 to 0.3 dex for PN and 0.1 to 0.2 dex for HII regions, especially for the elements with larger abundances, such as oxygen and nitrogen. The total PN sample includes over 1300 objects, while the HII region sample has over 900 objects, so that a reasonably large sample of Local Group objects is considered, amounting to over 2200 photoionized nebulae. Although not a complete sample, it is large enough to compensate for the inevitable degree of inhomogeneity, so that some interesting conclusions on the chemical evolution of the systems considered can be obtained. The data sources are partially listed by Maciel et al. (2014), with the addition of some recent data as discussed below.

New data on the chemical abundances of planetary nebulae (PN) in different systems have been obtained by our group. This sample is hereafter referred to as the IAG sample, and has important consequences for the nucleosynthesis of the PN progenitor stars and for the chemical evolution of the Galaxy (see for example Idiart et al. 2007, Costa et al. 2008, Maciel et al. 2009, 2010a, 2010b, Maciel & Costa 2009, Cavichia et al. 2010, 2011, 2017). These systems include the solar neighbourhood, the galactic disk, the galactic bulge and the Magellanic Clouds. Abundances of the main chemical elements have been determined, namely, He, N, O, Ne, S and Ar, and the derived abundances are expected to be correct to 0.2 to 0.3 dex on average. Most PN abundances considered here have been derived by the analysis of forbidden lines with the use of ionization correction factors (ICFs), and the reader is referred to the papers cited above for details on the adopted procedures.

Apart from our own data, we have considered some recent abundance determinations from the literature, particularly from sources using a procedure similar to that of our group, so that a direct comparison can be made for the objects in common.

Girard et al. (2007) analyzed a sample of 48 galactic PN with [WR] central stars, comprising [WC], [WO] and wels (weak emission line stars). In agreement with their own conclusions, we find no important differences between these objects and the "normal" PN, at least concerning the chemical abundances of the elements considered.

In a series of papers, Henry and collaborators (2000, 2004, 2010, 2012) and Milingo et al. (2010), established accurate abundances for a large sample of galactic PN, comprising objects in the galactic disk and anticenter, forming an extremely homogeneous sample. The methods used to determine the abundances were similar to ours, so that it is possible to compare the results of our group with these data, especially in view of our intended comparison with Local Group objects. Particularly important here is the discussion on the "sulphur anomaly", as

we will see in detail in the following section. We have also included the results of the very recent surveys by García-Hernández & Górny (2014) and Delgado-Inglada et al. (2015), based on Spitzer data. Comparisons of infrared data with optical spectroscopic data produce a particularly accurate set of abundances, as also discussed by García-Hernández et al. (2016). These investigations (see also Delgado-Inglada et al. 2014) have considerably improved the determination of the ICFs, which are an essential part of the abundance determinations in PN from forbidden lines. The uncertainties are then, in principle, smaller than in previous investigations, but in fact the derived abundances are comparable, so that we feel safe to include these results in the present investigation.

Apart from our own data on the Magellanic Clouds, we have included samples from Stasińska et al. (1998, SRM) and Leisy & Dennefeld (2006, LD). In agreement with some conclusions by Henry et al. (2010), part of the results by Leisy & Dennefeld (2006) are upper limits or overestimates, and have not been included in our sample. Our results can then be considered as an update and improvement over the results by Stasińska et al. (1998), where an attempt was made to compare the PN population in five galaxies: Milky Way, LMC, SMC, M31, and M32.

Abundances of a large sample of PN in the Galaxy (disk, bulge, and halo) and in the Magellanic Clouds were analyzed by Milanova & Kholtygin (2009). The similarity of the elemental abundances in these objects was pointed out, in agreement with our present results, taking into account the lower metallicities of the LMC and SMC. The average uncertainties in these abundance determinations are similar as in our data, typically of 0.1 dex for helium and 0.2 dex for the other elements. Finally, we have also used the compilation of PN data by Chiappini et al. (2009), who included objects in the galactic bulge and disk, as well as in the Large Magellanic Cloud. This is a particularly large sample, so that we could use it as a check of the consisitency of the abundances of the sources considered, in order to minimize the effects of the inhomogeneity of these sources.

The comparison samples of HII regions for the Milky Way and Magellanic Clouds are from Afflerbach et al. (1997), Guseva et al. (2007), Rudolph et al. (2006), Tsamis et al. (2003), and Delgado-Inglada et al. (2015). We have preferably adopted abundances determined from detailed electron temperatures, which are usually more accurate than the results from the strong line method. Some recent results by Reyes et al. (2015) for both clouds have also been taken into account. Additional data for HII regions in the Magellanic Clouds come from Peimbert et al. (2000), who presented chemical abundances for the HII region NGC 346 in the SMC based on spectrophotometric data obtained at the CTIO 4m telescope. We have here adopted the results for the preferred value of the fluctuation temperature parameter t^2, as given in their table 9. Also, Peña-Guerrero et al. (2012) presented chemical abundances of two HII regions in the SMC, NGC 456 and NGC 460, based on long-slit spectrophotometry taking into account the presence of thermal inhomogeneities. We have adopted here the average of the positions reported in the paper. Selier & Heydari-Malayeri (2012) presented chemical abundances of He, O, N, and Ne for two outer HII regions in the Magellanic Clouds, LMC N191 and SMC N77. The data were obtained by optical imaging and spectroscopic ESO NTT observations along with archive data. Finally, by combining optical and infrared data, Vermeij & van der Hulst (2002) determined element abundances for a sample of HII regions in the Large and Small Magellanic Cloud. We have considered 15 HII regions from their sample, with abundances of He, O, N, Ne, S, and Ar.

We have also included data on PN and HII regions in several external galaxies apart from the Magellanic Clouds, in order to compare them with the local data. Of course, as pointed out by Richer and McCall (2016), PN that are far away are selected among the brightest objects, so that it remains to be investigated whether or not these objects are representative of the PN population.

Kwitter et al. (2012) analyzed a sample of 16 PN in the outer disk of M31, for which they could derive electron temperatures and abundances. As we will see in the next section, our results agree with their conclusions, in the sense that the M31 PN display the same correlations as type II PN in the Galaxy. These results have been complemented with data on 2 PN by Balick et al. (2013). HII regions in this object have been analyzed by Zurita & Bresolin (2012), Sanders et al. (2012) and Esteban et al. (2009), usually by the direct method involving the determination of the electron temperature.

Richer & McCall (2008) studied a sample of 14 PN in M32, 4 PN in NGC 185 and 10 PN in NGC 205. Some enrichment was observed especially for N in the bright PN, suggesting that the main sequence mass of the PN progenitors was about $1.5 M_\odot$ or less.

TABLE 1

DATA FOR PLANETARY NEBULAE

	System	Number	Reference
1	MW disk	230	IAG
2	MW bulge	179	IAG
3	MW disk	22	Chiappini et al. (2009)
4	MW bulge	88	Chiappini et al. (2009)
5	MW	19	Girard et al. (2007)
6	MW	4	Henry et al. (2004)
7	MW	20	Henry et al. (2010)
8	MW	2	Milingo et al. (2010)
9	MW	6	Milanova & Kholtygin (2009)
10	MW	44	García-Hernández & Górny (2014)
11	LMC	251	IAG, SRM, LD
12	LMC	110	Chiappini et al. (2009)
13	LMC	14	Milanova & Kholtygin (2009)
14	SMC	129	IAG, SRM, LD
15	SMC	7	Milanova & Kholtygin (2009)
16	M31	1	Balick et al. (2013)
17	M31	16	Kwitter et al. (2012)
18	M32	14	Richer & McCall (2008)
19	M33	16	Bresolin et al. (2010)
20	M33	93	Magrini et al. (2009)
21	NGC 185	5	Richer & McCall (2008)
22	NGC 205	10	Richer & McCall (2008)
23	NGC 300	25	Stasińska et al. (2013)
24	NGC 3109	7	Peña et al. (2007)
25	Sextans	6	Magrini et al. (2005)

TABLE 2

DATA FOR HII REGIONS, BCG, AND ELG

	System	Number	Reference
1	MW	34	Afflerbach et al. (1997)
2	MW	53	Guseva et al. (2007)
3	MW	123	Rudolph et al. (2006)
4	MW	2	Tsamis et al. (2003)
5	MW	4	Delgado-Inglada et al. (2015)
6	MC	3	Tsamis et al. (2003)
7	MC	12	Reyes et al. (2015)
8	MC	1	Peimbert et al. (2000)
9	MC	2	Peña-Guerrero et al. (2012)
10	MC	2	Selier & Heydari-Malayeri (2012)
11	MC	15	Vermeij & van der Hulst (2002)
12	M31	1	Esteban et al. (2009)
13	M31	52	Sanders et al. (2012)
14	M31	9	Zurita & Bresolin (2012)
15	M33	3	Bresolin et al. (2010)
16	M33	2	Esteban et al. (2009)
17	M33	14	Magrini et al. (2007)
18	M33	60	Rosolowsky & Simon (2008)
19	M51	10	Bresolin et al. (2004)
20	M51	29	Croxall et al. (2015)
21	M81	12	Stanghellini et al. (2014)
22	M101	4	Esteban et al. (2009)
23	M101	20	Kennicutt et al. (2003)
24	NGC 300	28	Bresolin et al. (2009)
25	NGC 300	9	Stasińska et al. (2013)
26	NGC 628	45	Berg et al. (2015)
27	NGC 3109	10	Peña et al. (2007)
28	Sextans	17	Magrini et al. (2005)
29	BCG	54	Izotov & Thuan (1999)
30	ELG	306	Izotov et al. (2006)

For M33, Bresolin et al. (2010) obtained accurate abundances for 16 PN and 3 HII regions near the central parts of the galaxy. They found trends similar to those shown in section 3, including a comparison with BCG/ELG from Izotov et al. (2006). For this object, data from Magrini et al. (2009) for a large sample of PN were also considered. Also for HII regions, Magrini et al. (2007) presented data for 14 objects; two more objects come from the sample by Esteban et al. (2009), while Rosolowsky & Simon (2008) analyzed a larger sample of 60 HII regions with known oxygen abundances.

For M51, Bresolin et al (2004) presented a sample of 10 HII regions, and recent results by Croxall et al. (2015) have been taken into account. For M81 we have used HII region data by Stanghellini et al. (2014), and for M101 the HII region data by Kennicutt et al. (2003) and Esteban et al. (2009).

For NGC 300, Stasińska et al. (2013) analyzed a sample of PN and compact HII regions, and a similar sample of HII regions was taken from Bresolin et al. (2009) for this galaxy. For NGC 628 we have used recent data for a large sample of HII regions by Berg et al. (2015).

In the case of NGC 3109, Peña et al. (2007) studied a sample of PN and HII regions and concluded that the O and Ne abundances could be affected by the evolution of the PN central stars, although the size of the sample and the intrinsic uncertainties made this conclusion controversial. Finally, for the Sextans A and B galaxies, we used data by Magrini et al. (2005), who analyzed samples of PN and HII regions in these objects.

We also included in our analysis a sample of Blue Compact Galaxies and Emission Line Galaxies from Izotov and Thuan (1999) and Izotov et al. (2006), as they are equivalent of HII regions at relatively low metallicities (cf. Bresolin et al. 2010), as will be confirmed in the next section. These objects are essentially giant metal-poor HII regions, and fit nicely in the correlations obtained, but concentrate towards lower metallicities, $\log(\mathrm{O/H}) + 12 \leq 8.2$.

TABLE 3

TOTAL SAMPLES

PLANETARY NEBULAE	Number	HII REGIONS	Number
Milky Way Disk	347	Milky Way	216
Milky Way Bulge	267	Magellanic Clouds	35
Milky Way	614	Other Galaxies	325
Magellanic Clouds	511	BCG, ELG	360
Total External Galaxies	704	Total External Galaxies	720
TOTAL	1318	TOTAL	936

Tables 1 and 2 summarize the data for PN and HII regions, respectively, and Table 3 shows the total number of objects in each class.

3. RESULTS

3.1. *Elements not produced by the PN progenitor stars*

The abundances of the elements O, Ne, S, and Ar are probably not significantly affected by the evolution of the PN progenitor stars, and the corresponding distance-independent correlations are well determined. The measured abundances therefore reflect the interstellar abundances at the time the progenitor stars were born and can be compared with the data for the younger objects, such as HII regions.

3.1.1. *Oxygen*

Oxygen can be used as a metallicity proxy, and an accurate relation between O and Fe can be determined (see for example Ramírez et al. 2013). This is important, since in photoionized nebulae Fe is mostly locked up in grains. The average slope of the Fe - O correlation is approximately of 1.11 for the thin disk and 1.31 for the thick disk.

Figure 1 shows histograms of the oxygen abundance O/H for planetary nebulae and HII regions in three representative cases: The Mllky Way (top figures), the Milky Way and the Magellanic Clouds (middle figures) and all objects considered here, namely the Milky Way, the Magellanic Clouds and the remaining external galaxies (bottom figures). It can be seen that both PN and HII regions have similar distributions, peaking around $\log(\mathrm{O/H}) + 12 = 8.4$ to 8.8, although the HII region distributions are generally broader than in the case of planetary nebulae. Also, it can be noted that a larger fraction of HII regions have $\log(\mathrm{O/H}) + 12 \geq 9$, which reflects the fact that these younger objects are formed by more enriched material. Similar plots can be obtained for Ne, S, and Ar, although the samples are smaller than in the case of oxygen, since the abundances of these elements are usually more difficult to obtain. For the S/H ratio similar peaks are also observed for PN and HII regions in the three cases considered, but for Ne/H and Ar/H the total number of HII regions is relatively small, so that a comparison is difficult. An exception is the Ar/H histograms for all objects, which is similar to the results of Figure 1 (bottom).

In this paper we concentrate on distance-independent correlations, to avoid distance determination problems, which affect processes such as the abundance gradients observed in the Milky Way and other spirals. The main results are shown in Figures 2 to 10 for neon, sulphur, and argon, as functions of the oxygen abundance by number of atomos, O/H. The top figures show the abundances of these elements relative to hydrogen (Ne/H, S/H, and Ar/H), while the bottom figures show the abundances relative to oxygen (Ne/O, S/O, and Ar/O). In these figures, PN are always represented by empty symbols (squares and circles), while HII regions, BCG, and ELG are represented by triangles or crosses.

3.1.2. *Neon*

The results for Ne are shown in Figures 2, 3, and 4. Figure 2 shows the Milky Way objects, where the squares represent PN and the triangles represent HII regions. Bulge PN and disk PN have a similar behavior, so that they are both included as squares in the figure. In the top figure we see that for the Ne/H ratio both PN and HII regions present a lockstep variation with O/H, although for HII regions the dispersion is much smaller than for the case of planetary nebulae. This is also reflected in the bottom figure, which shows the Ne/O ratio as a function

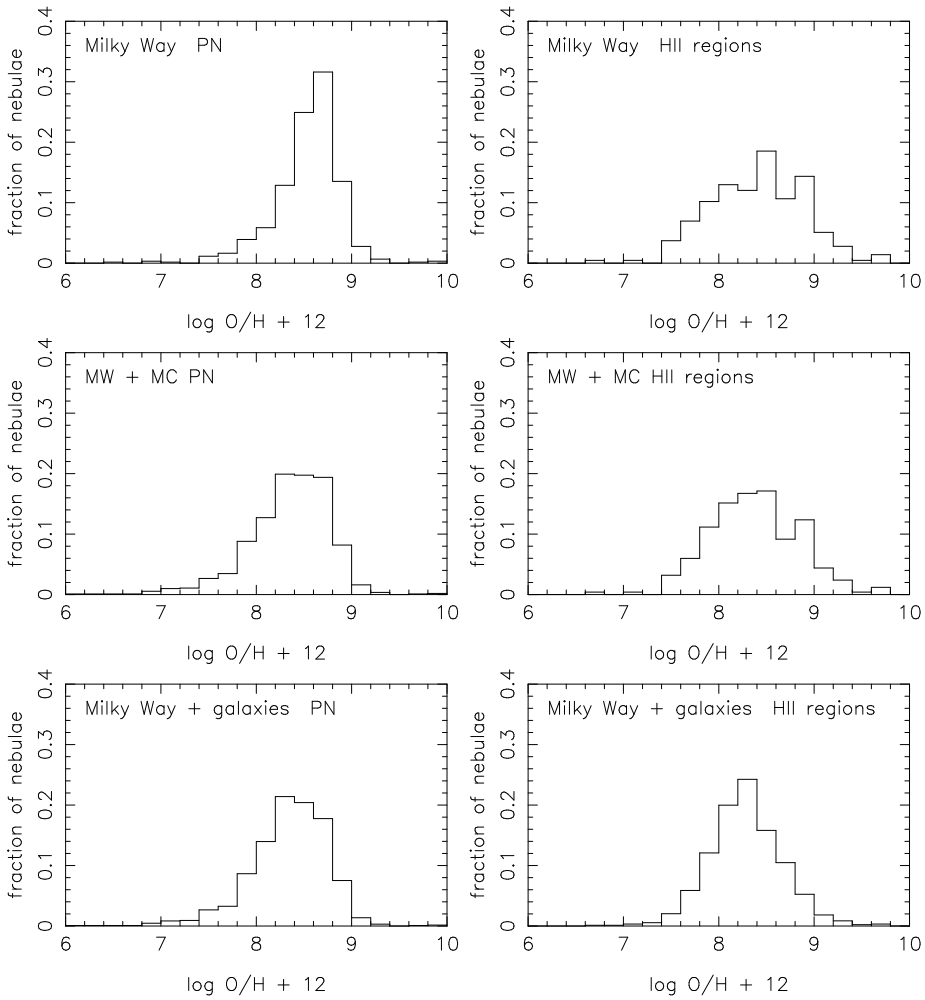

Fig. 1. Histograms of the O/H abundances in PN and HII regions. top: Milky Way; middle: Milky Way and Magellanic Clouds; bottom: Milky Way and all external galaxies.

of O/H, indicating that the Ne/O ratio is essentially constant with a higher dispersion for planetary nebulae. The estimated dispersions are given in Table 4 for the correlations of the abundances relative to hydrogen as functions of the O/H ratio.

Data for the Magellanic Clouds are included in Figure 3, where the squares are again PN in the Milky Way, the circles are PN in the Magellanic Clouds, the triangles represent HII regions in the Milky Way and the crosses are HII regions in the Magellanic Clouds. There is a well known metallicity difference between the LMC and SMC in the sense that the LMC has a higher average metallicity than the SMC, which is not shown in the figure, as both Clouds are represented by the same symbols. We can see that the same trend of Figure 2 is also apparent here, in the sense that the Ne abundances vary in lockstep with oxygen. A similar dispersion is observed for PN in both Figures 2 and 3. The MC data show a rather smooth transition to the Galaxy towards lower metallicities, which is especially noticeable in the PN data, where the separation of the MW PN and MC PN is more evident. The Magellanic Cloud PN are displaced towards lower Ne abundances, which reflects the lower metallicity of the Clouds relative to the Milky Way.

Data for the remaining external galaxies, comprising all galaxies in the Local Group, BCG, and ELG, are included in Figure 4. Here again MW PN are shown as squares, PN in external galaxies are shown as circles, MW HII regions are represented by triangles, and external HII regions are shown as crosses. It is remarkable that the same behavior observed in the Galaxy also holds in other Local

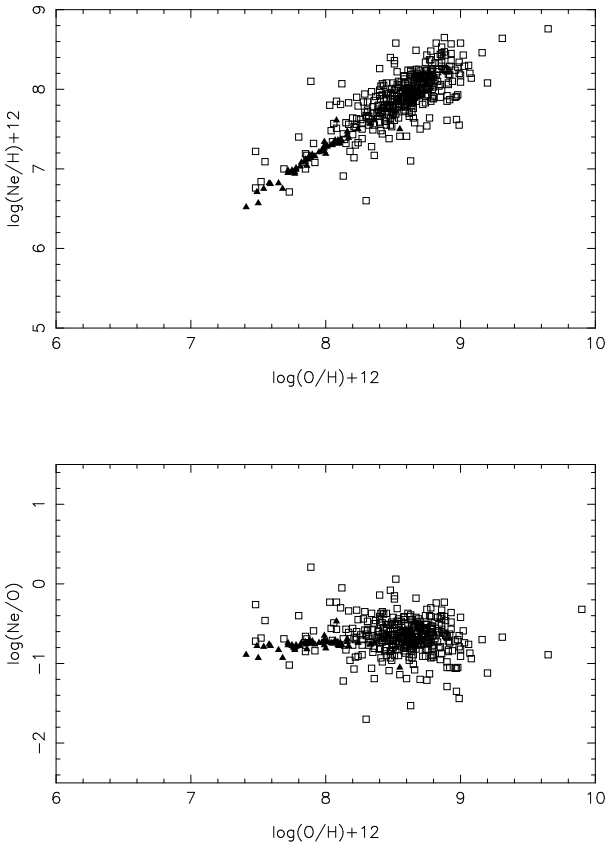

Fig. 2. Ne abundances as functions of oxygen abundances for the Milky Way: PN (squares), HII regions (triangles).

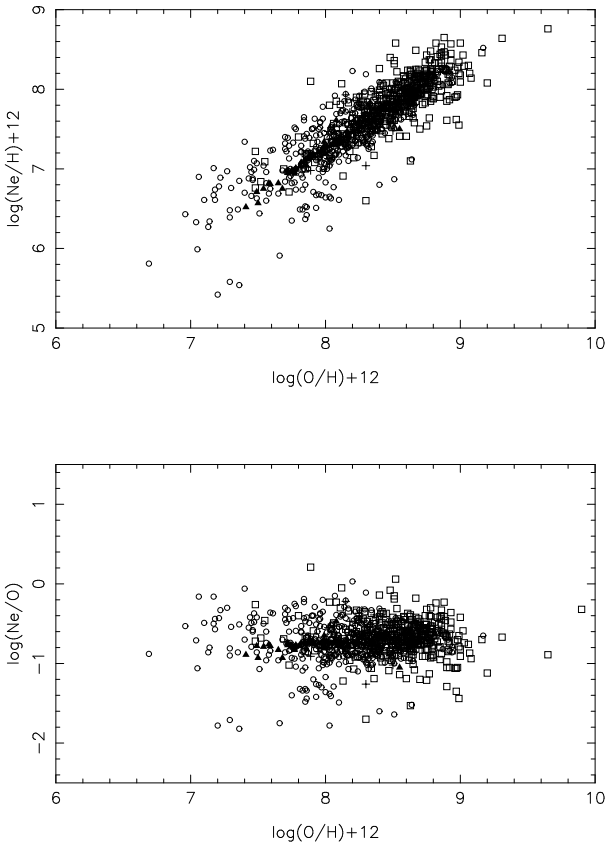

Fig. 3. The same as Figure 2 for the Milky Way and Magelllanic Clouds: MW PN (squares), MW HII regions (triangles), MC PN (circles), MC HII regions (crosses).

Group objects. Despite their different metallicities and morphologies, their nucleosynthetic processes and chemical evolution are apparently very similar. The trend displayed in Figure 4 (top) shows a very good agreement with the trend found by Izotov et al. (2006) on the basis of ELG only. Similar conclusions were obtained by Richer & McCall (2007, 2008). Even the average dispersions do not change appreciably for Local Group objects, and the lower dispersion in HII region abundances compared with PN has the same characteristics both in the Milky Way and in the Local Group objects. The fractions of objects within 1σ, 2σ, and 3σ are shown in Table 5, where both PN and HII regions are included.

It is also interesting to notice that in this larger sample the observed ranges of oxygen and neon abundances are similar, in spite of a few PN showing very high oxygen abundances. The similarity essentially reflects the fact that the interstellar metallicities did not change appreciably in the last 5 Gyr approximately, a result that is supported by recent determinations of the age-metallicity in the Milky Way (see for example Rocha-Pinto et al. 2000, Bensby et al. 2004a, 2004b). The abundances relative to oxygen shown in the bottom figure remain essentially constant, as in the case of Figures 2 and 3, but the dispersion of PN data is considerably higher.

The similarity of all photoionized nebulae coupled with the high dispersions shown by PN can be interpreted assuming that the dispersion in the PN data reflects the fact that the abundances are not as well determined as for the HII regions. However, a larger dispersion would be expected, since PN are older objects than the HII regions and any given sample probably includes objects of different ages, as we have shown elsewhere (Maciel et al. 2010a, 2010b, 2011). Apart from a few objects at very low metallicities, the same dispersion is observed at all metallicities, amounting to about 0.3 dex, considering also S and Ar. This is higher than, or similar to, the individual uncertainties in the abundances, so that the dispersion is probably real, reflecting the different ages of the PN central stars.

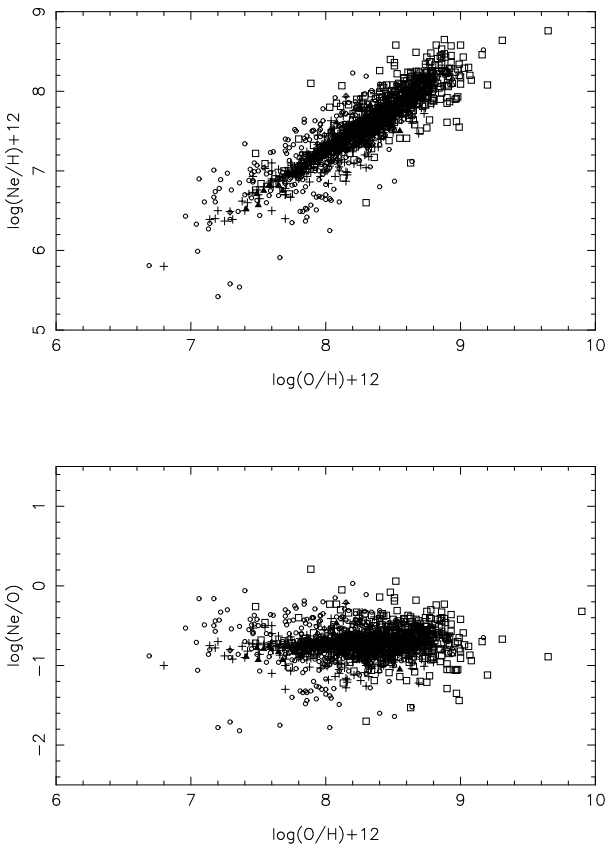

Fig. 4. The same as Figure 2 for the Milky Way and external galaxies: MW PN (squares), MW HII regions (triangles), external PN (circles), external HII regions (crosses).

Alternatively, it may be considered that there is some contribution to the Ne abundances from the PN progenitor stars, as suggested in some recent investigations (see for example Peña et al. 2007). Although oxygen and neon are mostly produced by the evolution of massive stars through core-collapse supernovae, some contribution from the PN progenitor stars is also supported by theoretical models. This interpretation, however, conflicts with the fact that the dispersion does not seem to change for different metallicities. If an important part of the Ne abundances were produced by the intermediate stars we would expect the dispersion to increase with the metallicity, which is not observed. Therefore, the most accurate data available for Ne do not suggest any important contribution from the PN progenitor stars, so that any such contribution would be expected to be smaller than the average uncertainties in the abundances.

It has been argued that the third dredge-up process in AGB stars may affect the oxygen abundances observed in planetary nebulae (see for example Karakas & Lattanzio 2014). ON cycling would also reduce the O/H ratio especially in lower metallicity PN. This appears to affect low metallicity objects with progenitor star masses higher than about

TABLE 4

AVERAGE DISPERSIONS AS FUNCTIONS OF O/H

	MW	MW+MC	ALL
N/H			
PN	0.42	0.48	0.38
HII regions	0.33	0.41	0.31
ALL	0.42	0.49	0.41
Ne/H			
PN	0.22	0.25	0.20
HII regions	0.09	0.15	0.13
ALL	0.21	0.24	0.16
S/H			
PN	0.33	0.38	0.27
HII regions	0.18	0.17	0.15
ALL	0.30	0.36	0.20
Ar/H			
PN	0.34	0.33	0.33
HII regions		0.11	0.17
ALL	0.34	0.32	0.24

TABLE 5

FRACTIONS OF OBJECTS WITHIN 1σ, 2σ, AND 3σ

	1σ	2σ	3σ
Ne/H			
Milky Way	0.75	0.94	1.00
MW + MC	0.77	0.94	1.00
MW + galaxies	0.78	0.93	1.00
S/H			
Milky Way	0.36	0.58	1.00
MW + MC	0.54	0.84	1.00
MW + galaxies	0.30	0.56	1.00
Ar/H			
Milky Way	0.41	0.67	1.00
MW + MC	0.54	0.85	1.00
MW + galaxies	0.44	0.73	1.00

$2M_{\odot}$ (see for example Karakas & Lattanzio 2007, Herwig 2005). Our results show that, if present, such contribution should be small compared with the average uncertainties in the PN abundances. Figures 2 to 4 show some evidence of this effect for $\log(\mathrm{O/H}) + 12 \leq 8$, but the number of PN at such low metallicities is a small fraction of the sample considered. It can be concluded that this effect, if present, is masked by the uncertainties in the abundance determinations, as well as by the different average metallicities of the objects considered here.

Taking into account the expected uncertainties in these abundances, an average contribution of about 0.1 dex cannot be ruled out. On the other hand, if we compare the expected contributions both to oxygen and neon, it is unlikely that they are equal, which is needed in order to explain the similarity of the PN and HII region trends shown in Figures 2 to 4 (cf. Karakas and Lattanzio 2003).

3.1.3. *Sulphur*

In the case of sulphur, as shown in Figures 5, 6, and 7, the general trends with oxygen are similar to neon, but some differences arise. The symbols are as in Figures 2, 3, and 4. For the Milky Way disk, the HII regions present a very good correlation, and the data extend to higher and lower metallicities compared with neon. The galactic PN already display what is usually called the "sulphur anomaly", that is, many PN apparently have somewhat lower S/H abundances than expected for their metallicity (see for example the detailed discussions by Henry et al. 2004, 2012); this can be observed in Figure 5 (top and bottom). The sulphur anomaly has been attributed to a deficiency in the calculation of the sulphur ICFs, particularly due to the abundance of the S^{+3} ion, to lack of accurate atomic constants, as an effect of the nucleosynthesis in the progenitor stars, and to a different chemical evolution of the systems considered. In Figure 5 it is clearly seen that more objects lie below the line defined by the HII regions, especially in the range $8.0 < \log(\mathrm{O/H}) + 12 < 9.0$.

Considering now the Milky Way and the Magellanic Clouds, we see in Figure 6, in which the symbols are as in Figure 3, that a new effect is apparent, in the sense that the S abundances in the Magellanic Clouds present a much wider dispersion than the galactic objects, showing many PN with higher sulphur abundances than the HII regions. There is still a reasonable number of objects below the HII region curve, but there is a large number of PN on the opposite side, so that the sulphur anomaly is not particularly noticeable, and in fact the data could be

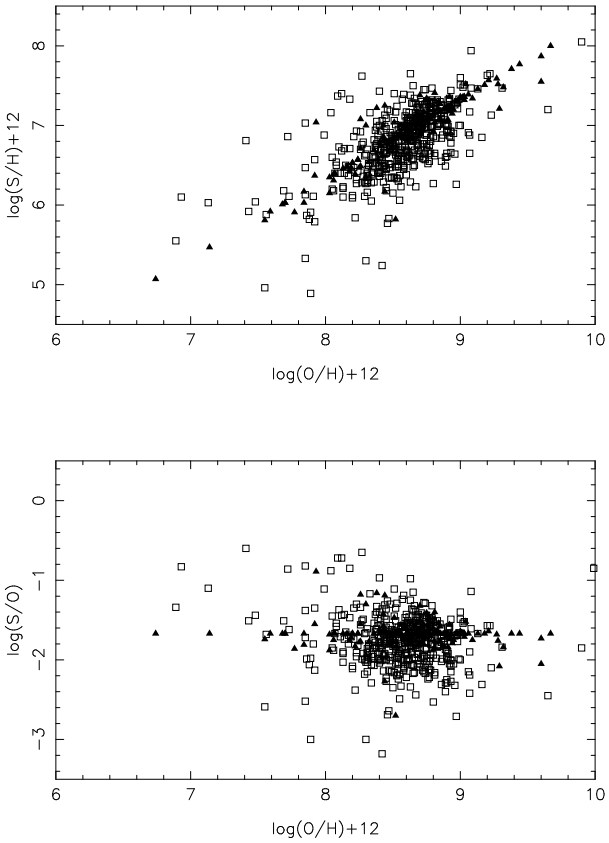

Fig. 5. The same as Figure 2 for sulphur.

attributed simply to the higher uncertainty for the MC abundances, suggesting that these abundances are not as well known as in the galactic PN.

Taking into account all objects in the Local Group, as shown in Figure 7, where the symbols are as in Figure 4, we see that the same general trends are maintained, with a higher dispersion compared with Ne for PN. It is noteworthy that for all HII regions, galactic as well as extragalactic, the lockstep variation with oxygen is very well defined, despite the fact that the objects considered are very different. Another consequence is that the sulphur anomaly becomes less important as additional samples are considered. This suggests that this problem is very probably related to the calculation techniques used to derive the sulphur abundances in galactic and possibly in Magellanic Cloud PN.

It can also be seen in Table 4 and Figures 5 to 7 that the average dispersion of the sulphur abundances is higher compared to Ne, and similar to the case of Ar, as we will see later on. For HII regions, essentially the same average dispersion is obtained in all cases. The inclusion of BCG and ELG maintains

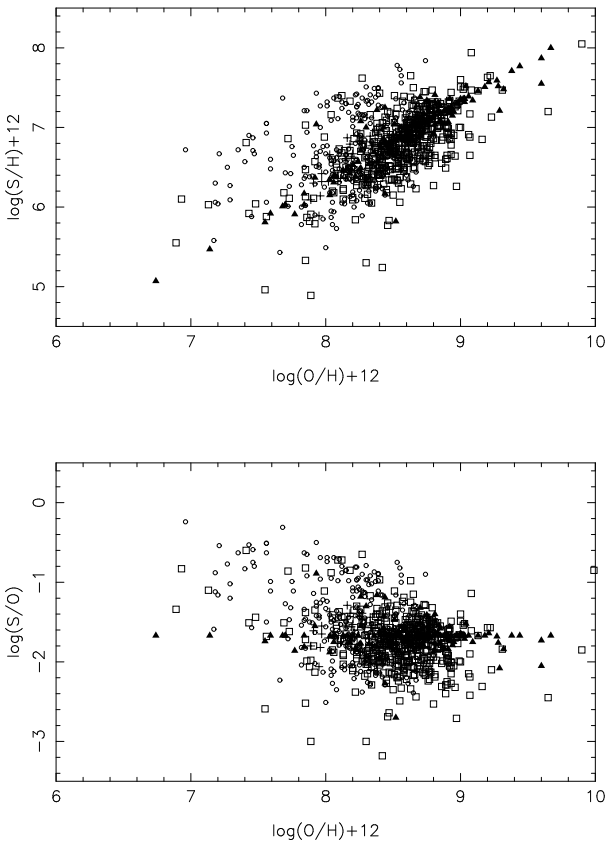

Fig. 6. The same as Figure 3 for sulphur.

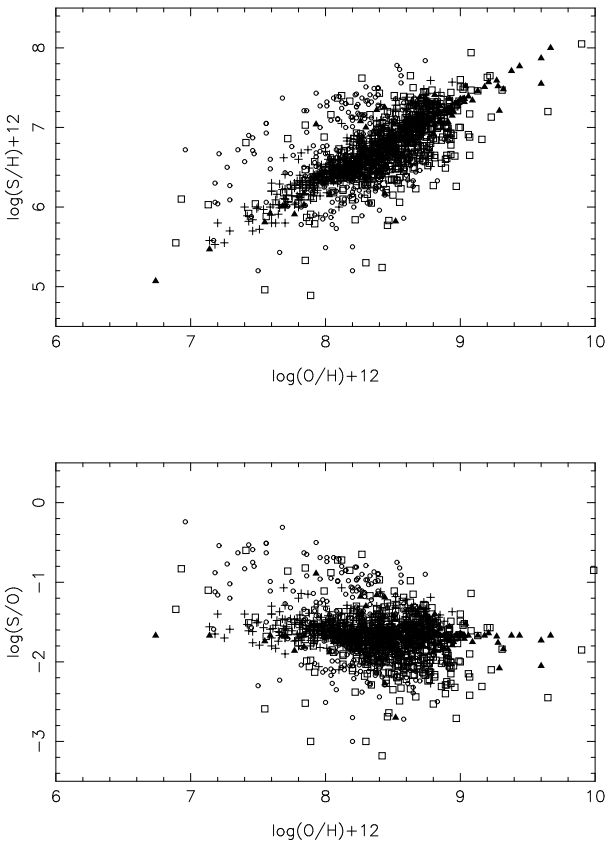

Fig. 7. The same as Figure 4 for sulphur.

these conclusions, that is, the sulphur abundances of HII apparently do not show the sulphur anomaly, which is then a characteristic of the empirical determination of sulphur abundances in planetary nebulae. In other words, the problem of the sulphur determinations affects basically the planetary nebulae, but not the HII regions or the blue compact galaxies.

As a conclusion, we see that the HII region trend is always well defined, while the PN data present at least three different problems: (i) the sulphur anomaly, apparent in galactic objects, (ii) a large number of objects with higher sulphur abundances compared with HII regions, especially in the Magellanic Clouds, and (iii) a higher dispersion in the PN data, compared to neon. Based on the estimates of the discrepancy in the sulphur abundances in the Clouds and in the Milky Way we suggest that the sulphur abundances of PN in the Clouds are probably overestimated up to a factor of the order of 3. Of course, the overestimate may be different for individual nebulae, so that this applies only to the bulk of the nebulae.

3.1.4. *Argon*

For argon the results are similar to those of neon, but the dispersion is higher, comparable to S/H, as can be seen in Table 4 and Figures 8, 9, and 10, again with the same symbols as in Figures 2 to 4. The comparison with HII regions suffers from the lack of data for this element, especially for the Milky Way, except when external galaxies are included, as shown in Figure 10. The inclusion of BCG and ELG clearly improves the correlation, showing that the correlation defined at higher metallicities for the Milky Way still holds for lower and intermediate oxygen abundances ($\log \mathrm{O/H} + 12 < 8.5$). It should be noticed here that although the Ar/H dispersion is higher for PN compared to the Ne abundances, in the case of HII regions it is essentially the same as for Ne/H and S/H, up to 0.2 dex, similar to the value of the uncertainty. Therefore, the HII regions are clearly more homogeneous than the PN, which reflects their very small ages, roughly a few million years. Clearly, within such a short time bracket the average interstellar abundances are not expected to change appreciably. The relatively small dispersion of the HII

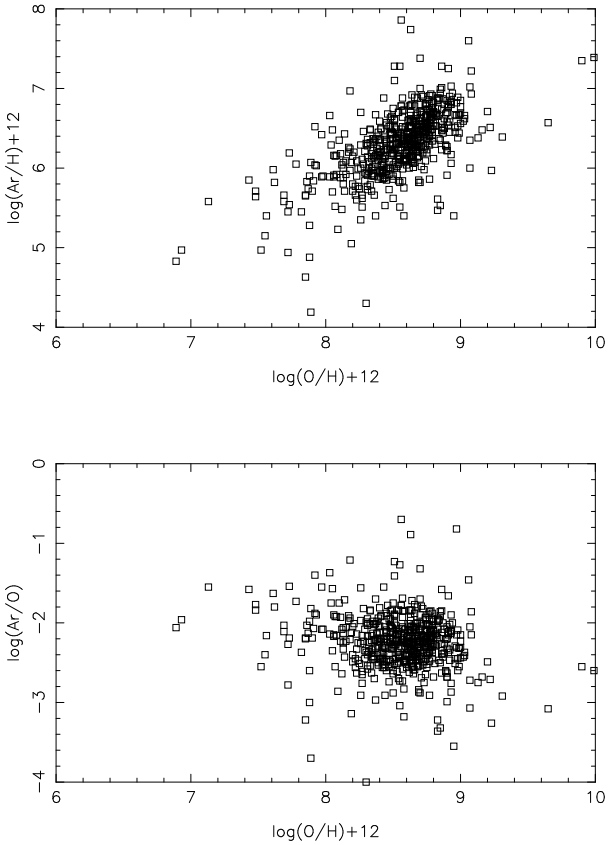

Fig. 8. The same as Figure 2 for argon.

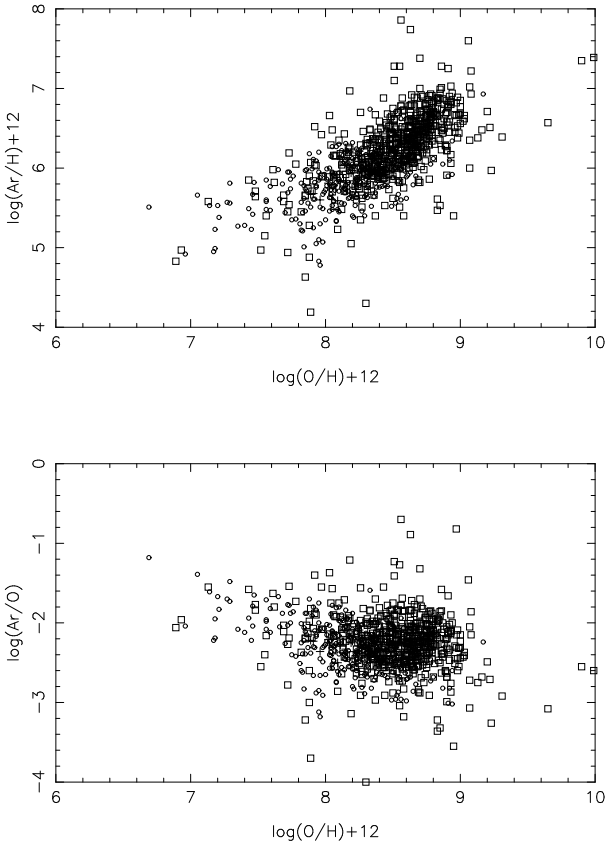

Fig. 9. The same as Figure 3 for argon.

region data for external galaxies can be understood in terms of the different metallicities of the Local Group objects. For PN, the dispersion in the data is considerably higher. As in the case of Ne, there is some evidence of a reduced oxygen abundance at lower metallicities.

3.2. *Elements produced by the PN progenitor stars*

In this work, we have stressed the elements that are not expected to be substantially produced by the PN progenitor stars, and we will present only a general outline of the elements that are strongly affected by the progenitor star evolution, such as He and N. Carbon abundances are also modified by the stellar evolution, but very few reliable carbon abundances for photoionized nebulae are presently available, so we will not consider this element here. The abundances of these elements are particularly modified by the dredge-up processes that occur in intermediate mass stars.

Histograms of the N/H abundances for PN and HII regions in our sample are shown in Figure 11, which can be directly compared with Figure 1. The PN distribution is similar in the three cases shown, and peaks around log(N/H) = 7.6 to 8.4, while for HII regions the same behavior is observed for the Milky Way and the Magellanic Clouds, but the inclusion of external galaxies (as well as BCG and ELG) shifts the maximum downwards by about 0.5 dex. The main difference between O/H and N/H, as shown in Figures 1 and 11, is that the nitrogen abundances extend to lower metallicities for HII regions compared with planetary nebulae, which reflects the N production during the evolution of the PN progenitor stars.

The main elements that are produced by the PN progenitor stars are He and N, for which there are generally good quality data for planetary nebulae and, to a lesser extent, for HII regions. Also, He determinations in HII regions are frequently affected by the presence of neutral helium, so that in this case the derived abundances are usually lower limits, which makes their analysis more difficult. In this work we have adopted a lower limit of He/H = 0.03 in order to avoid objects with an important fraction of neutral He.

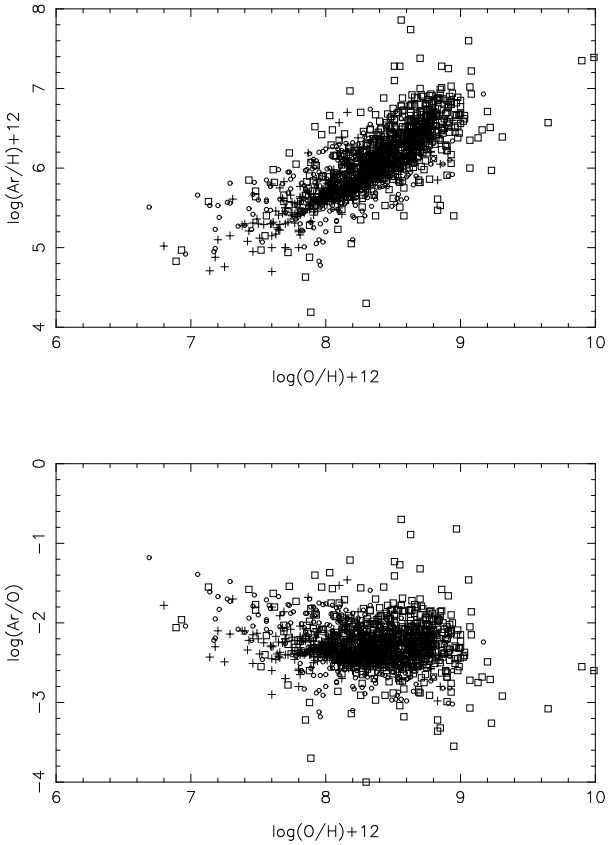

Fig. 10. The same as Figure 4 for argon.

Figure 12 shows the N/H and N/O ratios as functions of O/H and He/H, respectively, for the case where all objects are considered, namely, the Milky Way, the Magellanic Clouds, and external galaxies, keeping the same symbols as in Figure 4. This figure can be compared with the bottom Figures 4, 7, and 10 for Ne, S, and Ar, respectively. The most striking result is that, as expected, PN show an increase in both N and He compared to most HII regions in the sample. The average dispersions of the nitrogen data are also shown in Table 4, and it can be seen that they are much larger than in the case of Ne, S, and Ar, both for PN and HII regions. In other words, a larger dispersion is also observed for HII regions, so that part of their nitrogen is probably secondary. The excess nitrogen in PN is essentially produced by their progenitor stars, in a strong contrast with the remaining elements studied so far. The N/H ratio is roughly correlated with O/H in HII regions (Figure 12 top), but most PN are located above the average curve defined by the HII regions, again confirming the excess of N in planetary nebulae.

Considering now Figure 12 (bottom), it can be seen that there is a general trend for N/O with He/H in galactic as well as external planetary nebulae, but the dispersion is much higher than in the case of the previous plots, so that no definite correlation can be obtained, in agreement with similar conclusions by Richer & McCall (2008). Such a result clearly reflects the fact that the nitrogen abundances measured in planetary nebulae include both the pristine nitrogen plus the contribution from the dredge up processes that affect the red giant progenitor stars. Similar trends have also been recently discussed by García-Hernández et al. (2016), in a comparison of double-chemistry and oxygen-chemistry PN. It can also be seen in Figure 12 (bottom) that there are no important differences between galactic and external objects, and that the majority of PN have abundances close to solar, a result similar to the one obtained by Pottasch & Bernard-Salas (2010) for a smaller sample.

The N/O ratio shows some tendency to increase with the He abundances, indicating that both elements are produced in previous phases of the stellar evolution. Adopting a pregalactic He abundance by mass of about $Y = 0.255$ (cf. Izotov et al. 2014) which corresponds to approximately He/H = 0.09, we see in Figure 12 (bottom) that the PN enrichment is considerably larger than for HII regions, and that the difference between local and external PN is negligible. The cumulative distribution of the PN as a function of the He/H abundance is shown in Figure 13 (top). It can be seen that about 80% of the PN with He excess have abundances up to He/H $\simeq$ 0.141, a value about 57% higher than the pregalactic value. This can be compared with the value of 50% derived by Richer & McCall (2008) from a smaller sample. More recently, Lattanzio & Karakas (2016, see also Karakas & Lattanzio 2014) suggested an increase of about 38% in the helium content by mass from the second dredge-up process in AGB stars, which would lead to an increase of about 60% in the He abundance by number of atoms, in excellent agreement with the results shown in Figure 13.

Also from Figure 12 we can gain an idea of the amount of nitrogen produced by the progenitor stars. Adopting as limit for the primary nitrogen the amount produced by type II supernovae (Izotov et al. 2006), corresponding to approximately $\log \mathrm{N/O} = -1.6$, it can be seen that practically all PN are located way above this threshold. Considering the expected secondary nitrogen enrichment, which corresponds to about $\log \mathrm{N/O} = -1.2$, Figure 13 (bottom) shows that about 80% of the PN

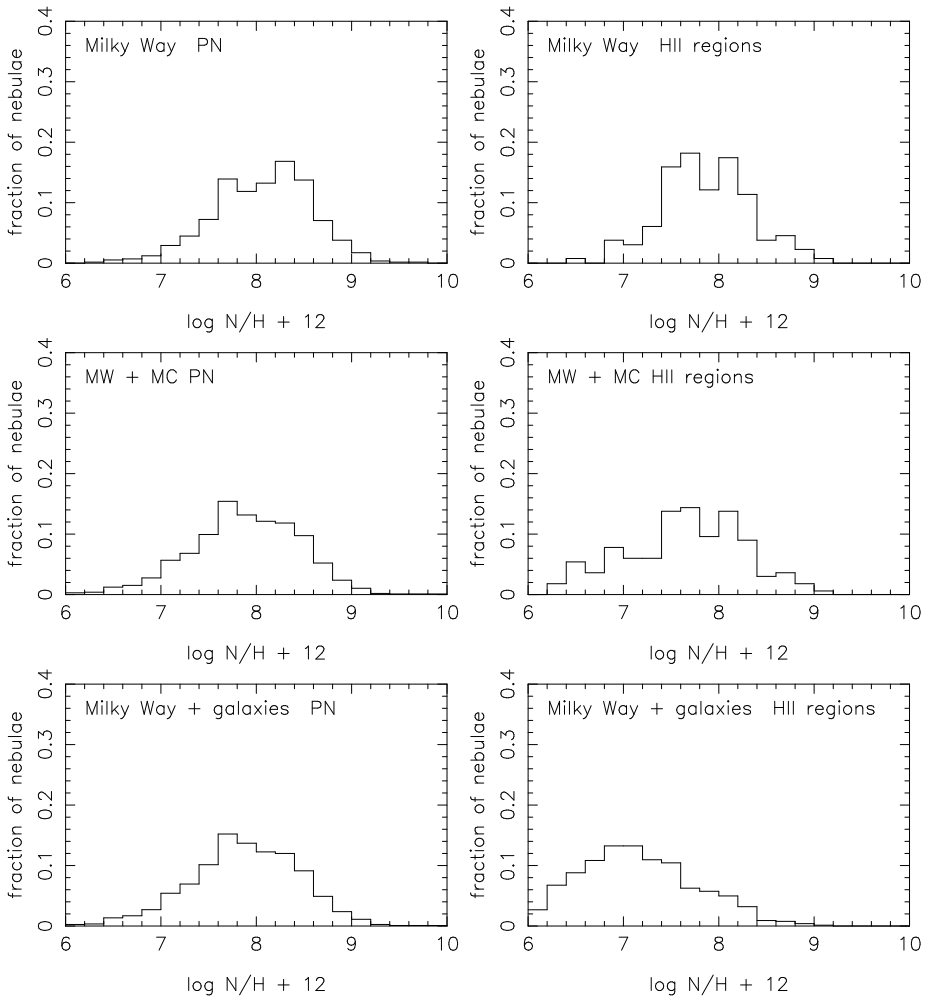

Fig. 11. Histograms of the N/H abudances in PN and HII regions. top: Milky Way, middle: Milky Way and Magellanic Clouds, bottom: Milky Way and all external galaxies.

present an enrichment ratio up to factor of 13.3, comparable with the factor of 10 found by Richer & McCall (2016).

In Figure 12 (bottom) we include a comparison with some recent theoretical models. The thick solid lines are taken from theoretical models by Karakas (2010, see also Karakas & Lattanzio 2007 and García-Hernández & Górny 2014), with $Z = 0.004$, 0.008, and 0.02, while the thick interrupted lines represent models by Marigo et al. (2003) with $Z = 0.019$. We have used straight lines to link the model results effectively obtained by Marigo et al. (2003) and Karakas (2010). These are synthetic evolutionary models for thermally-pulsating AGB stars with initial masses of 1 to 6 $M_{\odot}$, in which up to three dredge-up episodes occur, apart from hot-bottom processes (HBB) for the most massive objects. According to these models, progenitors having 0.9 to 4 $M_{\odot}$ and solar composition can explain the "normal" abundances, He/H < 0.15, while for objects with higher enhancements (He/H > 0.15), masses of 4 to 5 $M_{\odot}$ are needed, plus an efficient HBB. For intermediate mass stars, the agreement with theoretical models is fair, but abundance determinations should be improved and expanded. Recent models by Pignatari et al. (2016) with $Z = 0.01$ and 0.02 are also consistent with these results, as can be seen in the discussion by Delgado-Inglada et al. (2015). This paper also includes a discussion on the effects of different ICFs on the N and He production in the PN progenitor stars, as applied to a sample smaller than that considered here.

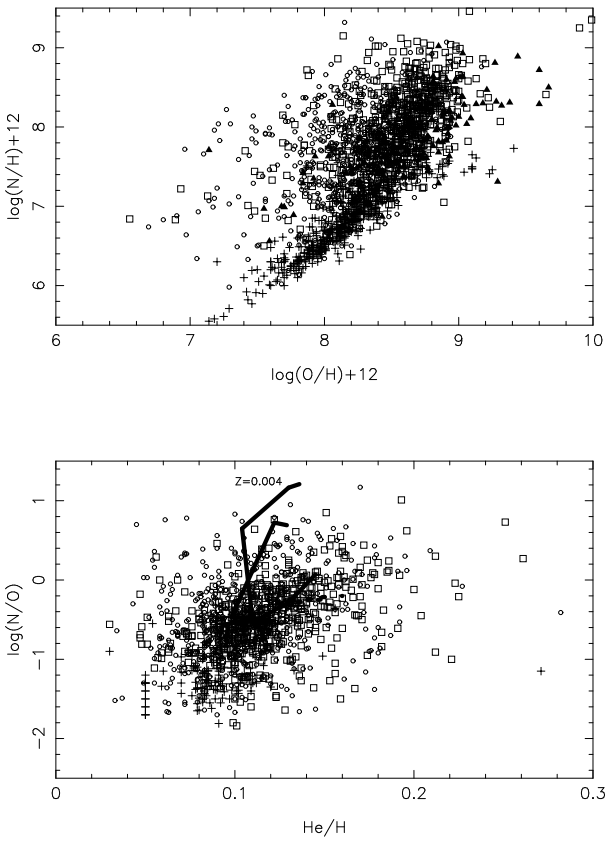

Fig. 12. Nitrogen abundances as functions of O/H (top) and He/H (bottom) for the Milky Way and external galaxies. MW PN (squares), MW HII regions (triangles), external PN (circles), external HII regions (crosses). In the bottom figure the thick solid lines represent models by Karakas (2010) for thermally pulsating AGB stars with Z = 0.004, as indicated at the top of the figure, and also for Z = 0.008 and Z = 0.02. The lower thick interrupted lines are models by Marigo et al. (2003) for Z = 0.019.

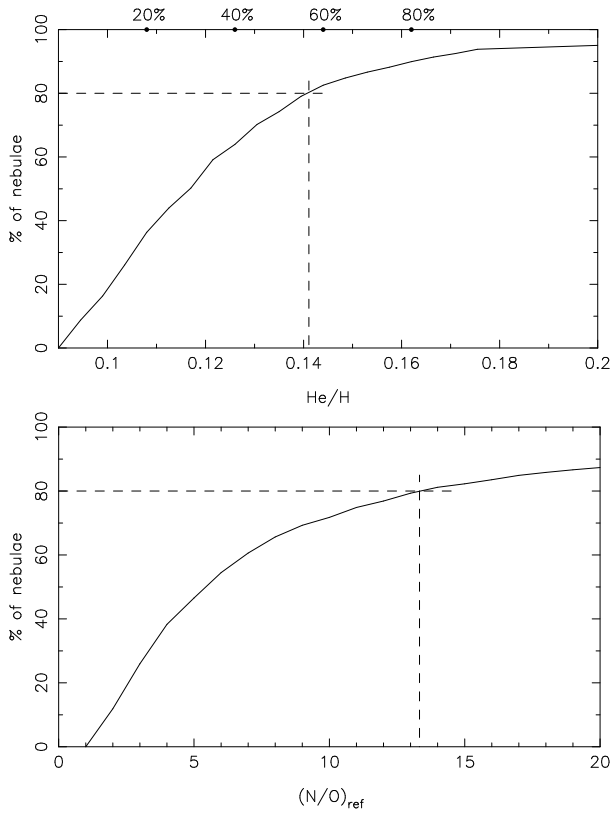

Fig. 13. Top: Cumulative distribution of PN as a function of the He/H abundance. About 80% of the nebulae have He/H lower than 0.141, as indicated by the dashed lines, which corresponds to a 57% enrichment relative to the reference value (He/H = 0.09). Bottom: Cumulative distribution of PN as a function of the N/O enrichment ratio. About 80% of the nebulae have an enrichment ratio of a factor 13.3 relative to the reference value (log N/O = –1.2), as indicated by the dashed lines.

4. CONCLUSIONS

The main conclusions of this paper are as follows:

• PN abundances of O, Ne, S, and Ar show good correlations, indicating that Ne, S, and Ar vary in lockstep with O. The correlations also apply to HII regions, BCG and ELG, but the dispersion is considerably lower for these objects.

• No important contribution to the Ne abundances from their progenitor stars is found in PN, so that any such contribution is probably lower than the current uncertainties in the abundance determination.

• For argon similar results as for neon are found, with a somewhat higher dispersion, probably due to the weakness of the Ar lines.

• Sulphur abundances in Milky Way PN may present the sulphur anomaly, that is, lower abundances than expected at a given metallicity. This anomaly is probably due to incorrect ICFs (ionization correction factors), but it is not apparent in the bulk of Local Group objects, for which a particularly extended metallicity range can be observed. The anomaly is not observed in MC PN, which show instead a larger dispersion than Milky Way objects. The dispersion observed in PN is probably real, and partially reflects the different ages of the progenitor stars. The variety of the sources considered may

also contribute to the observed dispersion, although an effort has been made to consider only works with similar approaches in the abundance determination.

• All correlations for HII regions show smaller dispersions, as expected, a result that is not affected by the inclusion of either BCG or ELG. The same trends are observed in both types of photoionized nebulae.

• Concerning planetary nebulae, it is interesting to notice that the average dispersion of the relations involving Ne, Ar, and S with oxygen is similar to that of the more homogeneous sample by Henry and co-workers, as can be seen for example in Milingo et al. (2010) (Here the remarks made on sulphur data are also applicable). This is very interesting, considering the fact that the Local Group galaxies have somewhat different metallicities, and possibly some differences in their chemical evolution processes. A similar result was obtained by Richer & McCall (2008) for neon. Also for neon and sulphur, results by Magrini et al. (2009) for M33 agree with the conclusions above. More recently, Richer & McCall (2016) pointed out that the relation of oxygen and neon abundances is similar to that of the star-forming galaxies, which again suggests that the PN progenitor stars either do not appreciably change the Ne abundances or the possible changes keep the original abundance ratio, implying progenitor masses of about 2 solar masses or less.

• The same mass interval is obtained from the comparison of the nitrogen abundances in PN with theoretical models of AGB stars, as PN have higher N and He abundances, and are located at the top right corner of the N/O vs. He/H plot. Therefore, these objects have originated from intermediate mass stars with masses typically under 2 $M_{\odot}$, except for the high He nebulae, whose progenitor stars are closer to the high mass bracket, around 4 $M_{\odot}$.

• A comparison of the N and He abundances in PN and HII regions shows that the former present an enrichment of these elements up to a factor of 13 for nitrogen and up to 57% for He, which agrees with some recent observational determinations as well as with theoretical models.

This work was partially supported by FAPESP and CNPq.

REFERENCES

Afflerbach, A., Churchwell, E., & Werner, M. W. 1997, ApJ, 478, 190
Balick, B., Kwitter, K. B., Corradi, R. L. M., & Henry, R. B. C. 2013, ApJ, 774, 3
Bensby, T., Feltzing, S., & Lundström, I. 2004a, A&A, 415, 155
_____. 2004b, A&A, 421, 969
Berg D. A., Croxall, K. V., Skillman, D. E., et al. 2015, ApJ, 806, 16
Bresolin, F., Garnett, D. R., & Kennicutt, R. C. 2004, ApJ, 615, 228
Bresolin, F., Gieren, W., Kudritzki, R. P., et al. 2009, ApJ, 700, 309
Bresolin, F., Stasińska, G., Vílchez, J. M., Simon, J. D., & Rosolowsky, E. 2010, MNRAS, 404, 1679
Cavichia, O., Costa, R. D. D., & Maciel, W. J. 2010, RMxAA, 46, 159
_____. 2011, RMxAA, 47, 49
Cavichia, O., Costa, R. D. D., Maciel, W. J., & Mollá, M. 2017, MNRAS (submitted)
Chiappini, C., Górny, S. K., Stasińska, G., & Barbuy, B. 2009, A&A, 494, 591
Costa, R. D. D., Maciel, W. J., & Escudero, A. V. 2008, BaltA, 17, 321
Croxall, K. V., Pogge, R. W., Berg D. A., Skillman, D. E., & Moustakas, J. 2015, ApJ, 808, 42
Delgado-Inglada, G., Rodríguez, M., Peimbert, M., Stasińska, G., & Morisset, C. 2015, MNRAS, 449, 1797
Delgado-Inglada, G., Morisset, C., & Stasińska, G. 2014, MNRAS, 440, 536
Esteban, C., Bresolin, F., Peimbert, M., et al. 2009, ApJ, 700, 654
García Hernández, D. A. & Górny, S. K. 2014, A&A, 567, A12
García Hernández, D. A., Ventura, P., Delgado-Inglada, G., et al. 2016, MNRAS, 461, 542
Girard, P., Köppen, J., & Acker, A. 2007, A&A, 463, 265
Guseva, N. G., Izotov, Y. I., Papaderos, P., & Fricke, K. J. 2007, A&A, 464, 885
Henry, R. B. C., Kwitter, K. B., & Balick, B. 2004, AJ, 127, 2284
Henry, R. B. C., Kwitter, K. B., & Bates, J. A. 2000, ApJ, 531, 928
Henry, R. B. C., Kwitter, K. B., Jaskot, A. E., et al. 2010, ApJ 724, 748
Henry, R. B. C., Speck, A., Karakas, A., Ferland, G. I., & Maguire, M. 2012, ApJ, 749, 61
Herwig, F. 2005, ARA&A, 43, 435
Idiart, T. E. P., Maciel, W. J., & Costa, R. D. D. 2007, A&A, 472, 101
Izotov, Y. I. & Thuan, T. X. 1999, ApJ, 511, 639
Izotov, Y. I., Stasińska, G., Meynet, G., Guseva, N. G., & Thuan, T. X. 2006, A&A, 448, 955
Izotov, Y. I, Thuan, T. X., & Guseva, N. G. 2014, MNRAS, 445, 778
Karakas, A. 2010, MNRAS, 403, 1413

Karakas, A. & Lattanzio, J. C. 2003, PASA, 20, 293
_____. 2007, PASA, 24, 103
_____. 2014, PASA, 31, 30
Kennicutt, R. C., Bresolin, F., & Garnett, D. R. 2003, ApJ, 591, 801
Kwitter, K. B., Lehman, E. M. M., Balick, B., & Henry, R. B. C. 2012, ApJ, 753, 12
Lattanzio, J. & Karakas, A. 2016, JPhCS, 728, 022002
Leisy, P., & Dennefeld, M. (LD) 2006, A&A, 456, 451
Maciel, W. J. & Costa, R. D. D. 2009, IAU Symp., 265, ed. K. Cunha, M. Spite, B. Barbuy
Maciel W. J., Costa, R. D. D., & Cavichia. O. 2014, PoS (NIC XIII), 030
Maciel, W. J., Costa, R. D. D., & Idiart, T. E. P. 2009, RMxAA, 45, 127
_____. 2010a, A&A, 512, A19
_____. 2010b, Nuclei in the Cosmos XI, PoS
Maciel, W. J., Rodrigues, T. S., & Costa, R. D. D. 2011, RMxAA, 47, 401
Magrini, L., Leisy, P., Corradi, R. L. M., et al. 2005, A&A, 443, 115
Magrini, L., Stanghellini, L., & Villaver, E. 2009, ApJ, 696, 729
Magrini, L., Vílchez, J., Mampaso, A., Corradi, R. L. M., & Leisy, P. 2007, A&A, 470, 865
Marigo, P., Bernard-Salas, J., Pottasch, S. R., Tielens, A. G. G. M., & Wesselius, P. R. 2003, A&A, 409, 619
Milanova, Yu. V. & Kholtygin, A. F. 2009, AstL, 35, 518
Milingo, J. B., Kwitter, K. B., Henry, R. B. C., & Souza, S. P. 2010, ApJ, 711, 619
Peimbert, M., Peimbert, A., & Ruiz, M. T. 2000, ApJ, 541, 688
Peña, M., Stasińska, G., & Richer, M. G. 2007, A&A, 476, 745
Peña-Guerrero, M. A., Peimbert, A., Peimbert, M., & Ruiz, M. T. 2012, ApJ, 746, 115
Pignatari, M., Herwig, F., Hirschi, R., et al. 2016, ApJS, 225, 24
Pottasch, S. R. & Bernard-Salas, J. 2010, A&A, 517, A95
Ramírez, I., Allende-Prieto, C., & Lambert, D. L. 2013, ApJ, 764, 78
Reyes, R. E. C., Navarro, A. R., Meléndez, J., Steiner, J., & Elizalde, F. 2015, RMxAA, 51, 133
Richer, M. G. & McCall, M. L. 2007, ApJ, 658, 328
_____. 2008, ApJ, 684, 1190
_____. 2016, Focus Meeting 4, XXIX IAU General Assembly, ed. P. Benvenuti (arXiv:1509.08537)
Rocha-Pinto, H. J., Maciel, W. J., Scalo, J., & Flynn, C. 2000, A&A, 358, 850
Rosolowsky, E. & Simon, J. D. 2008, ApJ, 675, 1213
Rudolph, A. L., Fich, M., Bell, G. R., et al. 2006, ApJS, 162, 346
Sanders, N. E., Caldwell, N., McDowell, J., & Harding, P. 2012, ApJ, 758, 133
Selier, R. & Heydari-Malayeri, M. 2012, A&A, 545, A29
Stanghellini L., Magrini, L., Cassola, V., & Villaver. E. 2014, A&A, 567, A88
Stasińska, G., Peña, M., Bresolin, F., & Tsamis, Y. G. 2013, A&A, 552, A12
Stasińska, G., Richer, M. G., & McCall, M. L. 1998, A&A, 336, 667
Tsamis, Y. G., Barlow, M. .J., Liu, X.-W., Danziger, I. J., & Storey, P. J. 2003, MNRAS, 338, 687
Vermeij, R. & van der Hulst, J. M. 2002, A&A, 391, 1081
Zurita, A. & Bresolin, F. 2012, MNRAS, 427, 1463

W. J. Maciel and R. D. D. Costa: Instituto de Astronomia, Geofísica e Ciências Atmosféricas, Universidade de São Paulo - Rua do Matão 1226, CEP 05508-090, São Paulo SP, Brazil (wjmaciel, roberto.costa@iag.usp.br).
O. Cavichia: Instituto de Física e Química, Universidade Federal de Itajubá, Av. BPS 1303, Pinheirinho, CEP 37500-903, Itajubá, MG, Brazil (cavichia@unifei.edu.br).